Chinese Chemical Letters 31 (2020) 2347–2352

Contents lists available at ScienceDirect

Chinese Chemical Letters

journal homepage: www.elsevier.com/locate/cclet

Communication

Bimetal-organic frameworks derived Co/N-doped carbons for lithium-sulfur batteries

Shifang Jiang[a], Shuo Huang[a], Minjie Yao[a], Jiacai Zhu[a], Lili Liu[b,*], Zhiqiang Niu[a,*]

[a] Key Laboratory of Advanced Energy Materials Chemistry (Ministry of Education), Renewable Energy Conversion and Storage Center, College of Chemistry, Nankai University, Tianjin 300071, China

[b] Tianjin Key Laboratory for Photoelectric Materials and Devices, School of Materials Science and Engineering, Tianjin University of Technology, Tianjin 300384, China

ARTICLE INFO

Article history:
Received 20 January 2020
Received in revised form 23 March 2020
Accepted 7 April 2020
Available online 14 April 2020

Keywords:
Lithium sulfur battery
Co/Zn-ZIF
Nitrogen-doped carbons
Catalyst
Separator modification

ABSTRACT

Lithium-sulfur (Li-S) batteries have received extensive attention due to their high theoretical specific energy density. However, the utilization of sulfur is seriously reduced by the shuttle effect of lithium polysulfides and the low conductivity of sulfur and lithium sulfide (Li_2S). Herein, we introduced bimetal-organic frameworks (Co/Zn-ZIF) derived cobalt and nitrogen-doped carbons (Co/N-C) into Li-S batteries through host design and separator modification. The Co/N-C in Li-S batteries effectively limits the shuttle effect through simultaneously serving as polysulfide traps and chemical catalyst. As a result, the Li-S batteries deliver a high reversible capacity of 1614.5 mAh/g and superior long-term cycling stability with a negligible capacity decay of only 0.04% per cycle after 1000 cycles. Furthermore, they have a high area capacity of 5.5 mAh/cm^2.

Lithium-sulfur (Li-S) batteries are considered as promising energy storage devices because of their high energy density (2600 Wh/kg) and large theoretical capacity (1675 mAh/g) [1,2]. Besides, the element sulfur is eco-friendly, natural abundance, and low-cost. However, the practical application of Li-S batteries is impeded by several drawbacks. For example, Li-S batteries often suffer from the sluggish conversion reaction in the charge/discharge process due to the insulating properties of sulfur and lithium sulfide [3]. Furthermore, the long-chain lithium polysulfides (LiPSs) is soluble in electrolyte and would migrate to lithium anode, resulting in the corrosion of the lithium metal anode and severe self-discharge [4]. As a result, the utilization of sulfur is severely limited, and the capacity, cycling life and coulombic efficiency of Li-S batteries rapidly degrade.

Recently, various strategies were developed to improve the electrochemical performance of Li-S batteries, such as sulfur host design [5–9], separator modification [10–15], electrolyte system innovation [16–18], as well as lithium anode protection [19–22]. Carbon materials are often utilized as the sulfur host and the active materials for modifying the separators due to their large surface area and high conductivity [23–25]. Unfortunately, the weak interaction between non-polar carbons and polar polysulfides would result in fast capacity decay over long-term cycling [26]. Thus, polar sites were introduced into carbon matrix by heteroatom doping (S, N, O, B, *etc.*) to enhance the chemisorption of nonpolar carbons for LiPSs [27–31]. Nevertheless, the chemisorption partially changes the chemical equilibrium of the sulfur species, and anchoring sites are limited [32]. Consequently, the shuttle of LiPSs is still occurred during charge/discharge process [33]. The sulfur redox reactions can be kinetically facilitated by an electrocatalysis to reduce the thermodynamic-driven LiPSs shuttle. Transitional metals (Co, Ni, Fe, *etc.*) are extensively applied in Li-S batteries because they can facilitate the formation or decomposition of Li_2S in the electrochemical processes [34–36]. Therefore, a novel strategy to obtain porous heteroatom-doped carbon materials with transitional metal nanoparticles would be desired for Li-S batteries.

Metal organic frameworks (MOFs) derived carbon materials have been used in Li-S batteries because of their highly uniform porosity and large surface area [37,38]. ZIF-67 derived cobalt and N-doped graphitic carbons can entrap polysulfides and catalyze sulfur redox synchronously [39,40]. However, ZIF-67 can only offer carbons with relatively lower nitrogen content and surface area than the case of ZIF-8 [41]. Combining the merits of ZIF-8 and ZIF-67, Co/Zn-ZIF derived carbons (Co/N-C) will possess large surface area, high conductivity, and highly dispersive N and Co-N active species, which are highly desired for the sulfur host in the cathodes and the active materials for modifying the separators [34,42,43]. Inspired by this, we prepared porous Co/N-C by calcining Co/Zn-ZIF

* Corresponding authors.
E-mail addresses: lililiuhappy@163.com (L. Liu), zqniu@nankai.edu.cn (Z. Niu).

http://dx.doi.org/10.1016/j.cclet.2020.04.014

at high temperature to serve as sulfur host as well as active materials for modifying separator. The electron-rich nitrogen atoms in Co/N-C can enhance the restriction of LiPSs *via* strong chemisorption and Co nanoparticles greatly accelerate the reversible conversion of intermediates during the charge/discharge process. As a result, the resultant Li-S batteries exhibit enhanced rate performance and excellent cycling stability.

$Zn(NO_3)_2{\cdot}6H_2O$ (6 mmol) and $Co(NO_3)_2{\cdot}6H_2O$ at a molar ratio of 4:1 were dissolved in 60 mL methanol, which was subsequently poured into 20 mL methanol containing 24 mmol 2-methylimidazole (2-MeIM). The mixture was standing for 24 h, resulting in the Co/Zn-ZIF. 600 mg Co/Zn-ZIF and 1.25 g 2-MeIM were well dispersed in 165 mL water and 105 mL methanol by ultrasonic dispersion. Then 5.5 mL cetyltrimethyl-ammonium chloride solution (CTAC, 25 wt% in H_2O) was injected into the solution. Subsequently, 8 mL tetraethyl orthosilicate (TEOS) was added into this mixture whine 5 min and stirred for another 1 h. The resulting core-shell nanoparticles (denoted as Co/ZnZIF@SiO_2) were collected and later dried under vacuum overnight. Then they were placed in a tube furnace and heated to 900 °C for 3 h under N_2 to obtain SiO_2@Co/N-C. To remove the SiO_2 shell, pyrolyzed samples were immersed in a certain amount of aqueous HF (10 wt%). The Co/Zn-ZIF without silicon shell was calcined at the similar condition. The final products were named as Co/N-C and Co/N-C-0, respectively.

Sulfur was encapsulated into Co/N-C *via* a melt-diffusion method, achieving Co/N-C@S [44]. The slurry of the Co/N-C@S, Super P, and polyvinylidene fluoride (PVDF) in N-methyl-2-pyrrolidone (NMP) with mass ratio 8:1:1 was coated onto aluminum foil and dried at 60 °C in a vacuum oven. The Super P@S electrodes were obtained by mixing sulfur powder, Super P and PVDF in NMP with mass ration of 7:2:1. The Co/N-C modified separator was prepared by coating slurry (mass ratio of Co/N-C, Super P and PVDF: 8:1:1) onto glass fiber and drying at 80 °C under vacuum.

Coin-type 2032 Li-S batteries were assembled in an Ar-filled glovebox (Mikrouna Universal 2440/750). Li metal foil with diameter of 12 mm and thickness of 0.3 mm was used as anode. The electrolyte is 1 mol/L lithium bis(trifluoromethanesulfomyl) in 1,2-dimethoxyethane and 1,3-dioxolane (1:1, v/v) with 1 wt% $LiNO_3$. The electrode area is 0.785 cm^2 and the areal sulfur loading is about 1.5 mg/cm^2. The amount of electrolyte is 25 μL/mg_s. XRD patterns were collected from Rigaku Smart Lab with Cu Kα radiation. The morphologies were characterized by field-emission SEM (JEOL JSM7500F, MERLIN Compact) and high-resolution transmission electron microscopy (HRTEM, FEI Talos F200×G2, AEMC) equipped with mapping images for elemental analysis. Raman spectra were recorded using a confocal Raman microscope (DXR, Thermo Fisher Scientific) with a 532 nm excitation from an argon-ion laser. The surface chemical composition was analyzed by X-ray photoelectron spectrometry (XPS; PerkinElmer PHI 1600 ESCA) with the bonding energy based on C 1s at 285 eV. The mass fraction of sulfur in the electrode was tested using a TG-DSC analyzer (NETZSCH, STA 449 F3) from room temperature to 500 °C with a heating rate of 5 °C/min in nitrogen atmosphere. Nitrogen adsorption isotherms were carried out at 77 K using a micromeritics ASAP 2020 analyzer. The adsorption experiment was performed by a Cary 60 UV-vis spectrophotometer (Agilent Technologies).

Fig. 1a schematically illustrates the experimental process of preparing the Co/N-C. Co/Zn-ZIF was simply synthesized by a similar strategy of preparing ZIF-8, where Co^{2+} partially replaces Zn^{2+} in ZIF-8 [42]. Co/Zn-ZIF displays similar shape and crystal lattices of ZIF-8 and ZIF-67, as reflected by the TEM image (Fig. 1b) and XRD patterns (Fig. S1 in Supporting information). Owing to the formation of C-N or C-C bonds, carbon materials obtained from MOFs by pyrolysis will suffer from irreversible fusion and aggregation of nanoparticles [45]. To avoid this problem, a SiO_2 shell with thickness of 60 nm was coated on the surface of Co/Zn-ZIF by hydrolyzing tetraethyl orthosilicate under alkaline environment, achieving Co/Zn-ZIF@SiO_2 architecture (Fig. 1c) [46]. Compared to the Co/N-C-0 that was directly derived from Co/Zn-ZIF without SiO_2 shell, Co/Zn-ZIF@SiO_2 architecture still nearly remain its initial structure after being pyrolyzed under N_2 at 900 °C due to the protection of SiO_2 shell, as shown in Fig. S2 (Suppporting information). Under such high temperature, the organic ligand 2-methylimidazole and the metal ions will be reduced to nitrogen-doped carbons and metal nanoparticles, respectively. The Zn nanoparticles will be further evaporated due to its low boiling point. Since the insulating of SiO_2 shell will limit the transfer of electrons and ions, SiO_2 shell was removed by immersing Co/Zn-ZIF@SiO_2 in HF solution overnight, obtaining the Co/N-C. As shown in Fig. 1d, Co/N-C has a porous structure and its pore size is about 2∼10 nm, leading to a large Brumaire-Emmett-Teller (BET) surface area of 1460.4 m^2/g and a high pore volume of 2.10 cm^3/g (Fig. 1h and Fig. S3 in Supporting information). They are beneficial for high sulfur loading and physical restriction for polysulfides. It is noted that cobalt was not entirely removed during the hydrofluoric acid etching process and there are Co nanoparticles smaller than 10 nm in the Co/N-C networks. They have a lattice spacing of 0.20 nm (Fig. 1e), which is in accord with the calculated value (2.05 Å) of the

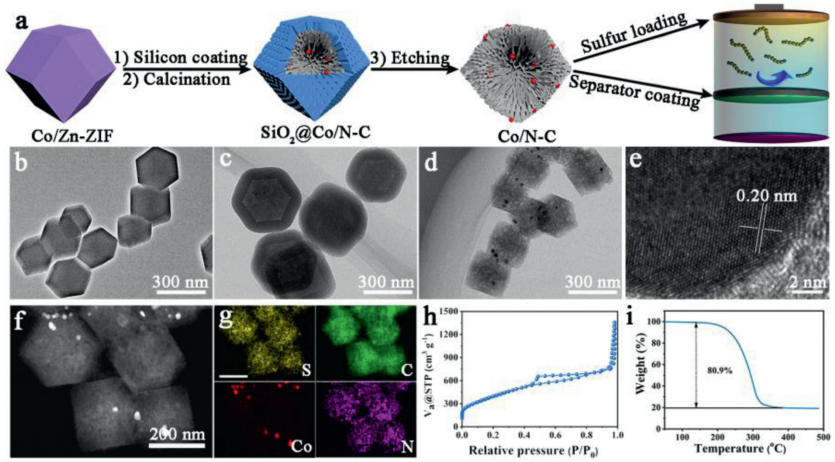

Fig. 1. (a) Schematic illustration of the synthesis procedure for Co/N-C. TEM images of (b) Co/Zn-ZIF, (c) SiO_2@Co/N-ZIF and (d) Co/N-C. (e) HRTEM images of Co/N-C. (f) HADDF-STEM image of Co/N-C@S. (g) The Co/N-C@S elemental mappings of S, C, Co and N. (h) N_2 adsorption-desorption analysis of the Co/N-C. (i) TG curve of Co/N-C@S.

(111) lattice facet of Co in the XRD patterns (Fig. S1) [47]. These results suggest that the Co^{2+} in Co/Zn-ZIF is reduced to Co nanoparticles and well disperse in the porous carbon matrix. Co nanoparticles can enhance the degree of graphitization of carbon matrix. Thus, Co/N-C displays high conductivity, which improves the electron transport properties of sulfur cathode. Apart from this, the carbon matrix is also doped by abundant nitrogen atoms (7.03 at%). The electronegative nitrogen would combine with Li^+ to form Li bond [30]. In addition, Co-N bonds exist in the Co/N-C, as revealed by both Co $2p_{3/2}$ and N 1s XPS spectra (Fig. S4 in Supporting information) [35]. They are efficient catalyst to accelerate the conversion of intermediate products for Li-S batteries [39].

Conductive networks acted as cathode host can accelerate electrons transfer, reducing the dissolution of LiPSs and relieving volume expansion during charge/discharge process. So, in order to introduce sulfur into the porous matrix, Co/N-C was mixed with sulfur and then heated at 155 °C. During this process, the sulfur was imbibed into the pores with the help of capillary forces and it is in intimate contact with the conductive Co/N-C matrix (Fig. 1f), obtaining Co/N-C@S. Owing to the large surface area and pore volume of Co/N-C, the loading of sulfur that can be encapsulated into Co/N-C reaches to 80.9 wt% (Fig. 1i). Besides, it is noted that no bulk sulfur particles aggregate on the surface of Co/N-C frameworks, as indicated by the transmission electron microscopy (TEM) images in Fig. 1f. It is also suggested by the Raman spectra (Fig. S5 in Supporting information) that sulfur signal of Co/N-C@S is not observed. Furthermore, the TEM element mappings (Fig. 1g) provide the evidence for the homogeneous distribution of sulfur in Co/N-C matrix. Remarkably, Co/N-C with high surface area, high conductivity and many polar sites is greatly suitable for the interlayer. Owing to the concentration gradient of LiPSs between anode and cathode, the dissolution and diffusion of LiPSs is unavoidable [52]. Therefore, a Co/N-C interlayer was introduced into Li-S batteries, which can absorb and restrain the migration of LiPSs, leading to the further conversion from soluble long-chain to insoluble short-chain, and efficiently increasing the sulfur utilization. Co/N-C was bladed on the glass fiber to modify separator. The Co/N-C layer is tightly adhered to the separator without any overpenetration and the thickness of the Co/N-C layer is about 19.0 μm (Fig. S6 in Supporting information).

To demonstrate the effectiveness of Co/N-C in immobilizing soluble intermediate products and accelerating their chemical conversion, Co/N-C was utilized to modify the separator and as sulfur host for coin-type Li-S batteries. Generally, the sulfur cathode goes through many reduction reactions, where the solid S_8 is firstly reduced to the soluble long-chain intermediates Li_2S_{4-8} and then to the short-chain Li_2S_2/Li_2S in discharge process. Correspondingly, there are two distinct reduction peaks at around 2.34 and 2.00 V in cyclic voltammetry (CV) curve in the voltage window 1.7-2.8 V at a scan rate of 0.1 mV/s (Fig. 2a). At the anodic scan, the broad oxidation peak at around 2.31 V is attributed to the oxidation process of lithium sulfide to sulfur. Impressively, the oxidation peaks of Li-S batteries with Co/N-C appear at lower potentials and display higher current intensity than the case of Li-S batteries without Co/N-C (2.51 V, Fig. S7 in Supporting information). Besides, the polarization potential of the batteries with Co/N-C is only 0.31 V, which is much lower than the case of Li-S batteries without Co/N-C (0.58 V), indicating much enhanced redox reaction kinetics of polysulfides. Moreover, the almost overlapping peaks in the initial five cycles indicate the good reversibility of the redox reaction in Li-S batteries with Co/N-C. In contrast, CV curves of the batteries without Co/N-C cannot overlap well and display dramatically polarizable redox peaks along with the increasing cycles. This suggests that the Co/N-C plays an important role in confining the shuttle effect and effectively enhancing the electrochemical kinetics process.

Since $LiNO_3$ additives in electrolyte to form a SEI layer that prevent lithium anode from being corroded by dissolved LiPSs, as a control experiment, the electrochemical performance of the Li-S batteries based on the electrolyte without $LiNO_3$ additive was measured [53]. With the help of Co/N-C, the Li-S batteries without $LiNO_3$ still exhibits a capacity of 1313.5 mA h/g with a sulfur loading of 1.5 mg/cm^2 (Fig. S8 in Supporting information), which is higher than the case of Li-S batteries without Co/N-C but with $LiNO_3$. It is further confirmed that the Co/N-C can effectively restrict the dissolution of the polysulfides *via* chemical interaction in the charge/discharge process. However, the capacity of the Li-S battery without $LiNO_3$ additive is lower than that of the battery with $LiNO_3$ additive. To guarantee the optimal electrochemical performance of Li-S batteries, the electrolyte with $LiNO_3$ additive was used in our work. As discussed above, Co/N-C can not only serve as the sulfur host, but also be used to modify the separators. When Co/N-C is only used as a host, Co/N-C@S electrode achieves an initial specific capacity of 1429.0 mA h/g at 0.1 C (1 C = 1675 mA/g) (Fig. 2c), which is much higher than the case of conventional super P@S electrode. When Co/N-C only serves as active materials of modifying separators, the batteries display a specific capacity of 1543.3 mA h/g at 0.1 C (1 C = 1675 mA/g), which is

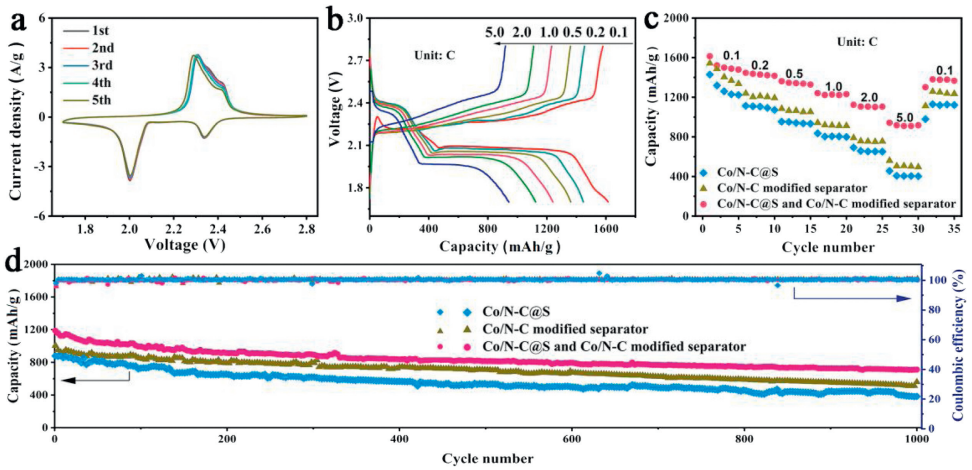

Fig. 2. (a) CV curves between 1.7 V and 2.8 V with a scan rate of 0.1 mV/s and (b) charge/discharge curves of Li-S batteries with Co/N-C@S and Co/N-C modified separator. (c) Rate performance and (d) cycling stability of Li-S batteries with different cathodes and separators.

also superior to the case with conventional separators. More impressively, combining the Co/N-C modified separator with the Co/N-C@S electrode, Li-S batteries achieve a high initial specific capacity of 1614.5 mA h/g at 0.1 C (Fig. 2b), which indicates the high sulfur utilization. Furthermore, even at a high current density of 5.0 C, they could deliver higher capacity of 942.2 mA h/g than the Li-S batteries only with Co/N-C modified separator or Co/N-C@S (560.5 and 490.9 mA h/g, respectively). When the current densities were returned to 0.1 C, they can still recover a high capacity of 1380.6 mA h/g. Moreover, even after 1000 charge/discharge cycles at 1.0 C, they can remain a reversible capacity of 711.2 mA h/g with 0.04% capacity decay per cycle. Furthermore, it is noted that the rate and cycling performance of Li-S batteries with Co/N-C@S cathode and Co/N-C modified separator are better than the cases of conventional Li-S batteries and Li-S batteries with Co/N-C@S cathode or Co/N-C modified separator (Figs. 2c and d, Fig. S9 in Supporting information,). Importantly, the electrochemical performance of the Li-S batteries with dual-functional Co/N-C (used as both cathode host and interlayer on separator) is superior to the previously reported works (Table S1 in Supporting information). These enhanced electrochemical properties are ascribed to the strong chemical interaction between Co/N-C and LiPSs as well as the accelerated conversion reaction of polysulfide intermediates.

Generally, pure carbon materials are non-polar while LiPSs is polar. As a result, their chemical interaction is very weak, resulting in fast capacity decay [48]. Thus, polar-polar chemical interaction is desired in Li-S batteries for long-term cycling. To understand the chemical interactions between Co/N-C and LiPSs, X-ray photoelectron spectroscopy (XPS) characterization was carried out (Fig. 3). In Li 1 s spectrum, Li-N bond is observed [49]. In addition, S 1 s spectrum reveals the existence of S-O and Co-S bonds at 169.0 and 169.6 eV, respectively [50]. These indicate the existence of strong chemical interactions between Co/N-C and LiPSs. When Co/N-C was added into bright yellow Li_2S_6 solution and stood for 12 h, the solution color changed to nearly transparent. Correspondingly, the characteristic peak of lithium polysulfides at 280 nm is very weak in UV-vis spectra [10]. But in the case of super P, the Li_2S_6 solution were still pale yellow. It indicates the strong chemical interactions between Co/N-C and LiPSs are achieved, which lead to the enhanced electrochemical performance of Li-S batteries with Co/N-C@S cathode or Co/N-C modified separator.

The electrochemical kinetic behavior of Li-S batteries depends on the introduction of Co/N-C. And the electrochemical kinetic behavior of Li-S batteries can be reflected by CV curves at different scan rates (Figs. 4a and b). CV curves show that the redox peaks gradually strengthen with the increasing scan rate from 0.2 mV/s to 1.0 mV/s. Their peak currents (i) and scan rates (v) have a relationship as below [51]:

$$i = av^b$$

where i, b, and v are peak current, kinetic parameter, and scan rate, respectively. In general, b-value of 0.5 would indicate that the conversion kinetic is controlled by semi-infinite linear diffusion and a value of 1 indicates that the conversion kinetic is surface-controlled. As shown in Fig. 4c, in the Li-S batteries with Co/N-C@S cathode and Co/N-C modified separator, the b values corresponding to peak 1, 2 and 3 are 0.493, 0.669 and 0.518, respectively. They are higher than the case of Li-S batteries without Co/N-C, suggesting a much faster electrochemical kinetics process (Fig. S10 in Supporting information). To confirm the electrocatalytic activity of Co/N-C, the symmetric cell was assembled by using the Co/N-C on steel mesh as both cathode and anode and Li_2S_6 solution as the electrolyte. Its CV curve displays a pair of reversible redox peaks at a scan rate of 100 mV/s (Fig. 4d). Since only Li_2S_6 is the active reactant, Li_2S_6 is reduced to lithium sulfide (Peak a) during discharge process. In the subsequent charge process, the lithium sulfide was reversibly oxidized to the final sulfur element (Peak b) [35]. In contrast, the symmetric cells with the Super P electrodes exhibit far lower current response without obvious redox peaks than the case of the Co/N-C electrodes. It indicates higher catalytic ability of the Co/N-C in the electrochemical process.

High sulfur loading is very essential for the practical applications of Li-S batteries [54]. However, it is always at the

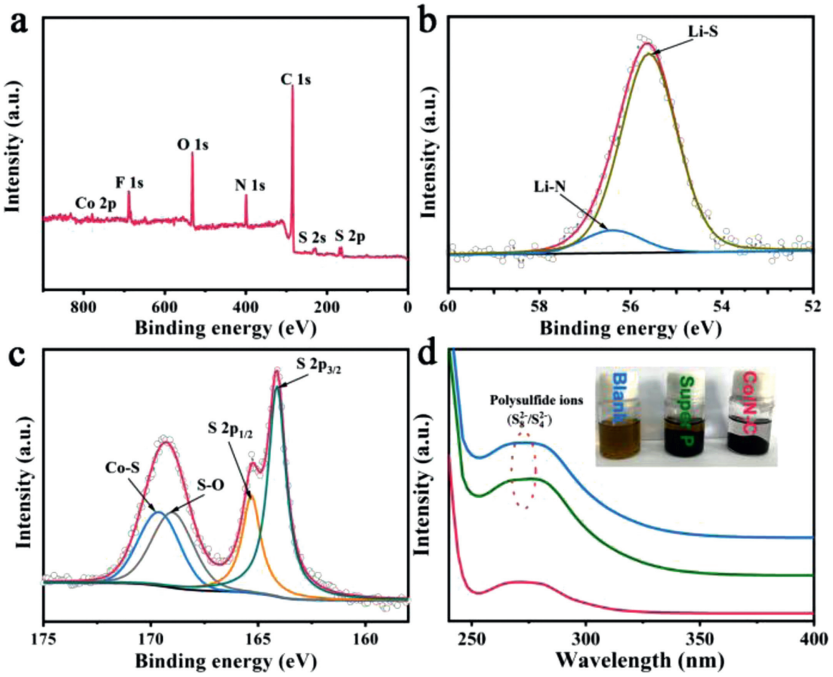

Fig. 3. (a) Total XPS spectra, (b) Li 1 s, (c) S 1 s of Co/N-C@S at discharge state of 2.1 V. (d) UV-vis adsorption spectroscopy of the pristine Li_2S_6 solution and the solution with 12 h static adsorption of Co/N-C and Super P.

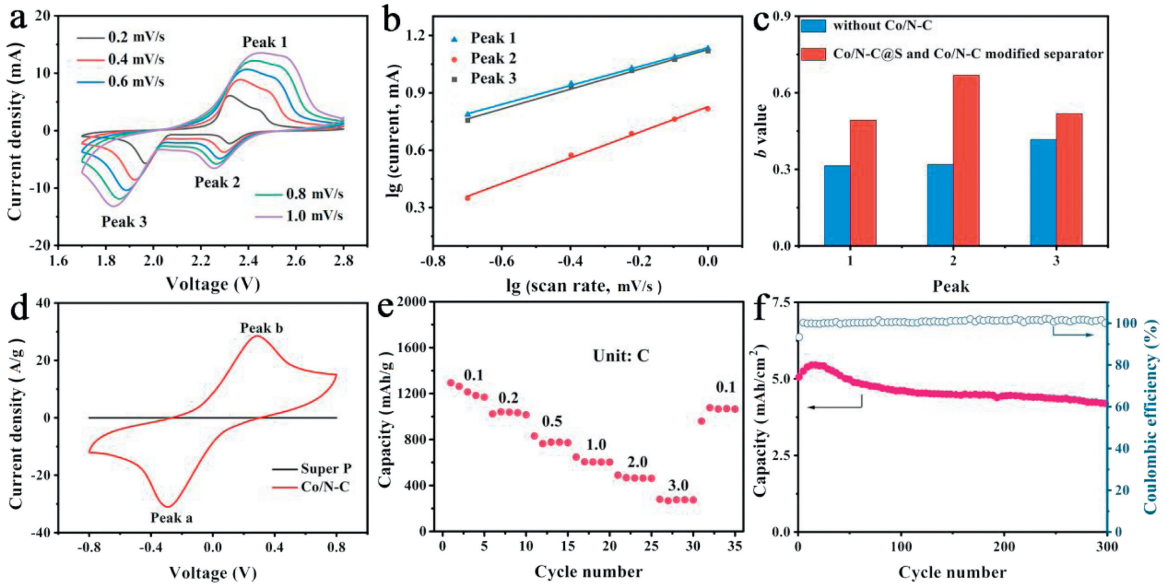

Fig. 4. (a) CV curves at different scan rates and (b) kinetics process (log(*i*) *versus* log(*v*) plot corresponding to redox peak (1-3)) of Li-S batteries with Co/N-C@S and Co/N-C modified separator. (c) The comparison of *b* values. (d) CV curves of symmetrical cells at a scan rate of 100 mV/s. (e) Rate performance and (f) cycling performance at 1.0 C of Li-S batteries with Co/N-C@S and Co/N-C modified separator with a sulfur loading of 6.0 mg/cm^2.

expense of rapid capacity decay and poor rate performance due to the failure of shuttle effect controlling and sluggish kinetics of batteries. High surface area and pore volume are very important for high sulfur loading and physical restriction for LiPSs. To enhance the kinetics of intermediate products, strong chemical interaction, and catalytic effect are obviously significantly. In our case, based on the Co/N-C coated separator and Co/N-C host simultaneously, Li-S batteries with a sulfur loading of 6.0 mg/cm^2 deliver 1292.9 mA h/g at 0.1 C and 279.2 mA h/g at 3.0 C (Fig. 4e). Moreover, they exhibit a large discharge area capacity of 5.5 mA h/cm^2 that is higher than the commercial lithium ion batteries (4.0 mA h/cm^2) and they can retain a capacity of 4.3 mA h/cm^2 after 300 cycles (Fig. 4f) [55]. Also, the coulombic efficiency that is close to 100% demonstrates that Co/N-C effectively limits the dissolution of the LiPSs and the shuttle effect even at a high sulfur loading. Therefore, Li-S batteries based on Co/N-C@S and Co/N-C modified separator exhibit superior rate performance and good cycling stability due to the physical and chemical restriction as well as catalytic effect of Co/N-C.

Porous Co/N-C architecture was prepared by calcining Co/Zn-ZIF at high temperature. Its architectures possess large surface area and high conductivity. Co nanoparticles exist in the carbon matrixes that are also doped by nitrogen atoms. Co/N-C can serve as sulfur host as well as active materials for modifying separator. The micro-mesoporous structure can physically restrict LiPSs dissolution. The electron-rich N atoms prefer to interact with Li^+, while Co nanoparticles would synchronously bond with the polysulfide anions through the strong chemical binding in the electrochemical process. Furthermore, Co/N-C can also accelerate the conversion of polysulfides. Hence, the Co/N-C in Li-S batteries plays an important role in confining the shuttle effect through simultaneously serving as polysulfide traps as well as chemical catalyst. As a result, the Li-S batteries deliver a high reversible capacity of 1614.5 mA h/g and superior long-term cycling stability with a negligible capacity decay of only 0.04% per cycle after 1000 cycles. Most importantly, apart from the high capacity retention, they have a high area capacity of 5.5 mA h/cm^2. Therefore, this work provides a promising strategy to achieve excellent electrochemical performance of Li-S batteries.

Declaration of competing interest

The authors declare that they have no known competing financial interests or personal relationships that could have appeared to influence the work reported in this paper.

Acknowledgments

This work was supported by National Natural Science Foundation of China (Nos. 51822205, 21875121, 51602218 and 51972231) Ministry of Science and Technology of China (No. 2017YFA0206700), Ministry of Education of China (No. B12015), Natural Science Foundation of Tianjin Municipal Science and Technology Commission (No. 18JCQNJC02400), the Science & Technology Development Fund of Tianjin Education Commission for Higher Education (No. 2017KJ248).

Appendix A. Supplementary data

Supplementary material related to this article can be found, in the online version, at doi:https://doi.org/10.1016/j.cclet.2020.04.014.

References

[1] J. Wang, Y.S. He, J. Yang, Adv. Mater. 27 (2015) 569–575.
[2] Y.X. Yin, S. Xin, Y.G. Guo, L.J. Wan, Angew. Chem. Int. Ed. 52 (2013) 13186–13200.
[3] X. Chen, L. Peng, L. Yuan, et al., J. Energy Chem. 37 (2019) 111–116.
[4] J.Q. Huang, T.Z. Zhuang, Q. Zhang, et al., ACS Nano 9 (2015) 3002–3011.
[5] J. Cao, C. Chen, Q. Zhao, et al., Adv. Mater. 28 (2016) 9629–9636.
[6] Y. Fu, Y.-S. Su, A. Manthiram, Angew. Chem. Int. Ed. 52 (2013) 6930–6935.
[7] T. Zhou, W. Lv, J. Li, et al., Energy Environ. Sci. 10 (2017) 1694–1703.
[8] B.Q. Li, S.Y. Zhang, L. Kong, et al., Adv. Mater. 30 (2018) 1707483.
[9] M. Zhao, H.J. Peng, J.Y. Wei, et al., Small Methods (2019) 1900344.
[10] L. Zhang, F. Wan, X. Wang, et al., ACS Appl. Mater. Interfaces 10 (2018) 5594–5602.
[11] L. Zhang, X. Chen, F. Wan, et al., ACS Nano 12 (2018) 9578–9586.
[12] J.Q. Huang, Q. Zhang, H.J. Peng, et al., Energy Environ. Sci. 7 (2014) 347–353.
[13] Z. Cheng, H. Pan, J. Chen, et al., Adv. Energy Mater. 9 (2019) 1901609.
[14] X. Tang, Z. Sun, H. Yang, et al., J. Energy Chem. 31 (2019) 119–124.
[15] R. Xu, Y. Sun, Y. Wang, et al., Chin. Chem. Lett. 28 (2017) 2235–2238.
[16] G. Zhang, H.J. Peng, C.Z. Zhao, et al., Angew. Chem. Int. Ed. 57 (2018) 16732-16736.
[17] Y.Z. Sun, J.Q. Huang, C.Z. Zhao, Q. Zhang, Sci. China Chem. 60 (2017) 1508–1526.

[18] A. Rosenman, R. Elazari, G. Salitra, et al., J. Electrochem. Soc. 162 (2015) A470–A473.
[19] N. Zhang, B. Li, S. Li, S. Yang, Adv. Energy Mater 8 (2018) 1703124.
[20] Q. Pang, A. Shyamsunder, B. Narayanan, et al., Nat. Energy (2018) 783–791.
[21] H. Wang, D.D. Yu, C.W. Kuang, et al., Chem 5 (2019) 313–338.
[22] M. Chen, L. Cheng, J. Chen, et al., ACS Appl. Mater. Interfaces 12 (2020) 3681–3687.
[23] K. Chen, J. Cao, Q. Lu, et al., Nano Res. 11 (2018) 1345–1357.
[24] G. Zhou, S. Pei, L. Li, et al., Adv. Mater. 26 (2014) 625–631.
[25] Y. Yang, C. Chen, J. Hu, et al., Chin. Chem. Lett. 29 (2018) 1777–1780.
[26] Q.P. Wu, X.J. Zhou, J. Xu, et al., J. Energy Chem. 38 (2019) 94–113.
[27] Y.P. Xie, H.W. Cheng, W. Chai, et al., Chin. Chem. Lett. 28 (2017) 738–742.
[28] J.L. Qin, M. Zhao, H. Yuan, J.Q. Huang, J. Energy Chem. 46 (2020) 199–201.
[29] S.K. Liu, X.B. Hong, Y.J. Li, et al., Chin. Chem. Lett. 28 (2017) 412–416.
[30] T.Z. Hou, W.T. Xu, X. Chen, et al., Angew. Chem. Int. Ed. 56 (2017) 8178–8182.
[31] H.J. Peng, Q. Zhang, Angew. Chem. Int. Ed. 54 (2015) 11018–11020.
[32] B.Q. Li, H.J. Peng, X. Chen, et al., CCS Chem. 1 (2019) 128–137.
[33] J. Liu, W. Li, L. Duan, et al., Nano Lett. 15 (2015) 5137–5142.
[34] J. Xie, B.-Q. Li, H.-J. Peng, et al., Adv. Mater. 31 (2019) 1903813.
[35] L. Zhang, D. Liu, Z. Muhammad, et al., Adv. Mater. 31 (2019) 1903955.
[36] Z. Liu, L. Zhou, Q. Ge, et al., ACS Appl. Mater. Interfaces 10 (2018) 19311–19317.
[37] H.L. Jiang, B. Liu, Y.Q. Lan, et al., J. Am. Chem. Soc. 133 (2011) 11854–11857.
[38] G. Xu, B. Ding, L. Shen, et al., J. Mater. Chem. A 1 (2013) 4490–4496.
[39] Y.J. Li, J.M. Fan, M.S. Zheng, Q.F. Dong, Energy Environ. Sci. 9 (2016) 1998–2004.
[40] X.J. Zhou, J. Tian, J.L. Hu, C.L. Li, Adv. Mater. 30 (2018) 1704166.
[41] H.B. Wu, S. Wei, L. Zhang, et al., Chem. Eur. J. 19 (2013) 10804–10808.
[42] Y.Z. Chen, C. Wang, Z.Y. Wu, et al., Adv. Mater. 27 (2015) 5010–5016.
[43] B.Q. Li, L. Kong, C.X. Zhao, et al., InfoMat 1 (2019) 533–541.
[44] Q. Xiao, G. Li, M. Li, et al., J. Energy Chem. 44 (2020) 61–67.
[45] L. Shang, H. Yu, X. Huang, et al., Adv. Mater. 28 (2016) 1668–1674.
[46] Z. Li, H.C. Zeng, J. Am. Chem. Soc. 136 (2014) 5631–5639.
[47] Y. Li, J. Fan, J. Zhang, et al., ACS Nano 11 (2017) 11417–11424.
[48] Q. Pang, J. Tang, H. Huang, et al., Adv. Mater. 27 (2015) 6021–6028.
[49] J. Song, M.L. Gordin, T. Xu, et al., Angew. Chem. Int. Ed. 54 (2015) 4325–4329.
[50] J. Xu, W. Zhang, Y. Chen, et al., J. Mater. Chem. A 6 (2018) 2797–2807.
[51] V. Augustyn, J. Come, M.A. Lowe, et al., Nat. Mater. 12 (2013) 518–522.
[52] L. Fan, M. Li, X. Li, et al., Joule 3 (2019) 361–386.
[53] W. Li, H. Yao, K. Yan, et al., Nat. Commun. 6 (2015) 7436–7444.
[54] Z. Yuan, H.-J. Peng, J.-Q. Huang, et al., Adv. Funct. Mater. 24 (2014) 6105–6112.
[55] F. Pei, L. Lin, D. Ou, et al., Nat. Commun. 8 (2017) 482.